Arab J Sci Eng (2014) 39:3181–3189
DOI 10.1007/s13369-013-0886-5

RESEARCH ARTICLE - MECHANICAL ENGINEERING

Eulerian–Lagrangian Numerical Scheme for Contaminant Removal from Different Cavity Shapes

Nor Azwadi Che Sidik · Mehran Salehi

Received: 1 June 2012 / Accepted: 15 November 2012 / Published online: 8 November 2013
© King Fahd University of Petroleum and Minerals 2013

Abstract In the present article we present computational investigations of fluid–solid interaction flow. Such fluid–solid interaction flow was created in three different cavity shapes on the floor of a horizontal channel. The flow and solid particle dynamics were explored using cubic interpolated pseudo-particle method and Lagrangian scheme of Newton's law, respectively, for two objectives. The first is to demonstrate the validity of the proposed Eulerian–Lagrangian in predicting the main characteristics of fluid–solid interaction flow. The second objective is to shed light on the dynamics of the solid particle that are present in the three types of cavities, which has not been fully covered in the literature. The results show that the particles' trajectories are critically dependent on the magnitude of Reynolds numbers and the vortex behavior in the cavity. We also found that the highest rate of removal occurs in the early penetration of flow into the cavity, especially for the triangular cavity. Good comparisons with the previous studies demonstrate the multidisciplinary applications of this scheme.

Keywords Eulerian–Lagrangian · Solid particle · Cubic interpolated pseudo particle · Channel flow

الخلاصة

نعرض في هذه المقالة التحقيقات الحسابية لتدفق السائل - الصلب المتفاعل. وتدفق السائل - الصلب المتفاعل مثل هذا قد تم إنشاؤه في ثلاثة أشكال تجويف مختلفة على أرضية قناة أفقية. وتم استكشاف ديناميكيات التدفق والجسيمات الصلبة باستخدام طريقة شبه الجسيم ذي تحريف مكعب (CIP) ونظام لاغرانج من قانون نيوتن على التوالي لتحقيق هدفين. الأول للتدليل على صحة طريقة أولر - اغرانج المقترحة في التنبؤ بالخصائص الرئيسية لتدفق السائل - الصلب المتفاعل، والهدف الثاني لتسليط الضوء على ديناميكيات الجسيمات الصلبة التي تجري في ثلاثة أنواع من التجاويف التي لم يتم تغطيتها بالكامل في الأدب. وتبين النتائج أن مسارات الجزيئات تعتمد بشكل كبير على حجم أعداد رينولدز وسلوك الدوامة في التجويف. وقد جدنا أيضا أن أعلى معدل إزالة يحدث في الاختراق المبكر للتدفق إلى التجويف، وبخاصة بالنسبة للتجويف الثلاثي. وتثبت المقارنات الجيدة مع الدراسات السابقة تطبيقات متعددة التخصصات لهذا النظام.

1 Introduction

Knowledge of the flow over an open cavity is central in many natural and industrial applications. Examples are a car sunroof, an aircraft weapon bay, a landing gear well, etc [1–3]. Comprehending the major mean fluid flow phenomena, such as vortex strength and structure, is crucial for the environmental management and design and operation of such engineering equipment. A major limitation, in the problem of fluid flow over a cavity, is the insufficient information about the vortex structure due to the inflow velocity and also the shape of the cavity. Although there are few fundamental experimental investigations which dictate that the formation of a vortex enhances the mixing process and a strong vortex helps in the process of contaminant removal, more detailed phenomena such as the interaction between the vortex formation and the percentage of contaminant removal and flow parameters on the particle's dynamics are still not fully understood. Although not extensive, Table 1 shows the breadth of

N. A. Che Sidik (✉) · M. Salehi
Faculty of Mechanical Engineering, Universiti Teknologi Malaysia, 81310 UTM Johor Bahru, Malaysia
e-mail: azwadi@fkm.utm.my

Table 1 Selection of studies on flow over cavities

Authors	Flow	Cavity geometry	Method
Mesalhy et al. [4]	Turbulent	Rectangular cavity	Experimental and numerical
Zdanski et al. [5]	Laminar and turbulent	Rectangular cavity	Numerical
Kang and Sung [6]	Turbulent	Rectangular cavity	Experimental
Ozalp et al. [7]	Turbulent	Rectangular triangular Semicircular cavities	Experimental
Li et al. [8]	Laminar and turbulent	Rectangular cavity	Numerical
Arlindo et al. [9]	Thermal, turbulent	Square cavity	Numerical
Striba [10]	Thermal, laminar	Cubic cavity	Numerical
Yapici et al. [11]	Viscoelastic, laminar	Square cavity	Numerical
Yang et al. [12]	Laminar	Rectangular cavity	Numerical
Ekmekci et al. [13]	Turbulent	Rectangular cavity	Experimental
Zaki et al. [14]	Thermal, laminar	Conical cavity	Experimental
Fang et al. [15]	Laminar, particulate flow	Rectangular cavity	Experiment and numerical
Patil et al. [16]	Laminar	Rectangular cavity	Numerical
Stiriba et al. [17]	Thermal, laminar	Cubic cavity	Numerical

parameters which have been considered by previous studies on flow over cavities.

Most of the previous studies focussed on the flow over a square or rectangular cavity, although the cavities may be non-rectangular in applications. Ozalp et al. [7] studied the flow structure past a rectangular, triangular and semicircular cavity experimentally using particle image velocimetry (PIV) technique. Another experimental study was conducted by Zaki et al. [14] to investigate the mass transfer inside conical cavities for the purpose of understanding the rate of diffusion inside the cavities.

Although there are some reports on non-rectangular cavities, the complicated nature of the flow needs further investigations on various parameters which influence the flow characteristics inside cavities.

On the other hand, hydrodynamic cleaning of components, parts and pipelines has become widely accepted as an alternative method of cleaning process. However, other problems arise with the presence of distinct cavities and steps due to poorly fitted components or connections in the pipelines. These problems contributed to the accumulation of contaminants and cleaning of these can lead to quite difficult problems. Formation of recirculating vortices in cavities or steps can either enhance or prevent the removal of contaminant and depend on various flow parameters and characteristics of the contaminant itself. In order to highlight the relevance of the present work, a brief review of the major efforts describing the cleaning process is presented.

Until present day, only a few papers have been reported to experimentally investigate this kind of engineering process. It is believed that the main reason of lacking of experimental research on this kind of fluid–solid interaction phenomenon is the complicated nature of the problem. The size of the contaminants can be as big as pebbles or very tiny such as dust pollutant. To the best of the authors' knowledge, only Tsorng et al. [18] reported details of experimental results on the behavior of contaminants in lid-driven cavity flow from micro to macro sized particles. Other experimental works are Adrian [19], Han et al. [20], Matas et al. [21], Ushijima and Tanaka [22], Ide and Ghil [23], Hu [24], Liao [25]. However, according to these papers, high accuracy of laser equipment together with a high-speed digital image capture and data interpretation system is required to obtain reliable experimental data. High cost experimental devices such as these will not be affordable if not supported by research funds.

The computational efforts to study fluid–solid (a contaminant is considered a solid particle) interaction are rather few as well. Until now, only Kosinski et al. [26,27] provides extensive numerical results on the subject. From the behavior of one particle in a lid-driven cavity flow to thousands of particles in an expansion horizontal pipe has been studied in their research. This work sheds new hope in understanding this problem. Kosinski et al. applied the combination of continuum Navier–Stokes equations to predict fluid flow and Newton's second law for solid particles. Recently, Kosinski and Hoffmann [28] extended their investigations into the effects of collisions between solid particles to predict the formation of agglomerates.

Definitely, a proper numerical model is required to predict the interaction between the fluid and solid particle. With a precise treatment, the trajectory of a solid particle in a complex fluid structure, which will be demonstrated in this paper, can be reproduced at a certain level of accuracy.

There are two major objectives of the present article. The first is to propose a numerical scheme for the present case. The second objective is to shed light on the dynamics of the contaminants that are present in the three types of cavities, which has not been fully covered in the literature. The numerical scheme is first described and then the computational model results are presented and discussed. The parameters of major concern herein are the vortex structure and the rate and percentage of contaminant removal from three different cavity shapes on the floor of a horizontal channel. In this simulation, we consider very tiny micro particles and their density are the same as those of the fluid. Therefore, the buoyancy and gravitational forces can be neglected.

2 The Numerical Scheme

In the present study, the flow is considered isothermal, incompressible and in the laminar region. Therefore, the governing vorticity and vorticity transport equations can be expressed as follows

$$\omega = -\left(\frac{\partial^2\psi}{\partial x^2} + \frac{\partial^2\psi}{\partial y^2}\right) \tag{1}$$

$$\frac{\partial\omega}{\partial t} + u\frac{\partial\omega}{\partial x} + v\frac{\partial\omega}{\partial y} = \upsilon\left(\frac{\partial^2\omega}{\partial x^2} + \frac{\partial^2\omega}{\partial y^2}\right) \tag{2}$$

Before considering any numerical solution to the above set of equations, it is convenient to rewrite the equations in terms of dimensionless variables. The following dimensionless variables will be used here

$$\Psi = \frac{\psi}{u_\infty D}, \Omega = \frac{\omega D}{\upsilon}$$
$$U = \frac{u}{u_\infty}, V = \frac{v}{u_\infty}$$
$$X = \frac{x}{D}, Y = \frac{y}{D}, \tau = \frac{tu_\infty}{D} \tag{3}$$

In terms of these variables, Eqs. (1) and (2) become

$$\frac{\partial\Omega}{\partial\tau} + U\frac{\partial\Omega}{\partial X} + V\frac{\partial\Omega}{\partial Y} = \frac{1}{Re}\left(\frac{\partial^2\Omega}{\partial X^2} + \frac{\partial^2\Omega}{\partial Y^2}\right) \tag{4}$$

$$\Omega = -\left(\frac{\partial^2\Psi}{\partial X^2} + \frac{\partial^2\Psi}{\partial Y^2}\right) \tag{5}$$

Here, the dimensionless parameters of Reynolds number are defined as

$$Re = \frac{u_\infty D}{\upsilon} \tag{6}$$

3 Modeling Strategy

Cubic interpolation profile method (CIP) was proposed and has been highly proven to be a universal solver for hyperbolic type of equations [29–31]. The CIP is known as a numerical method for solving the advection term with low numerical diffusion. This method constructs a solution inside the grid cell close enough to the real solution of the given equation [32].

To see the treatment of CIP on the stream function formulation, we begin by recalling Eq. (4) and its spatial derivatives, and split them into advection and non-advection phases as follows

Advection phase:

$$\frac{\partial\Omega}{\partial\tau} = -\left(U\frac{\partial\Omega}{\partial X} + V\frac{\partial\Omega}{\partial Y}\right) \tag{7}$$

$$\frac{\partial\Omega_X}{\partial\tau} = -\left(U\frac{\partial\Omega_X}{\partial X} + V\frac{\partial\Omega_X}{\partial Y}\right) \tag{8}$$

$$\frac{\partial\Omega_Y}{\partial\tau} = -\left(U\frac{\partial\Omega_Y}{\partial X} + V\frac{\partial\Omega_Y}{\partial Y}\right) \tag{9}$$

Non-advection phase:

$$\frac{\partial\Omega}{\partial\tau} = \frac{1}{Re}\left(\frac{\partial^2\Omega}{\partial X^2} + \frac{\partial^2\Omega}{\partial Y^2}\right) \tag{10}$$

$$\frac{\partial\Omega_X}{\partial\tau} = \frac{1}{Re}\left(\frac{\partial^3\Omega}{\partial X^3} + \frac{\partial^3\Omega}{\partial X\partial Y^2}\right) - \frac{\partial U}{\partial X}\frac{\partial\Omega}{\partial X} - \frac{\partial V}{\partial X}\frac{\partial\Omega}{\partial Y} \tag{11}$$

$$\frac{\partial\Omega_Y}{\partial\tau} = \frac{1}{Re}\left(\frac{\partial^3\Omega}{\partial X^2\partial Y} + \frac{\partial^3\Omega}{\partial Y^3}\right) - \frac{\partial U}{\partial Y}\frac{\partial\Omega}{\partial X} - \frac{\partial V}{\partial Y}\frac{\partial\Omega}{\partial Y} \tag{12}$$

where $\Omega_X = \partial\Omega/\partial X$ and $\Omega_Y = \partial\Omega/\partial Y$

In the CIP method, the advection phase of the spatial quantities in the grid interval is approximated with a constrained polynomial using the value and its spatial derivative at neighboring grid points. The proposed cubic polynomial is expressed as

$$F_{i,j}(X,Y) = \left[\left(a_1\tilde{X} + a_2\tilde{Y} + a_3\right)\tilde{X} + a_4\tilde{Y} + \Omega_X\right]\tilde{X} + \left[\left(a_5\tilde{Y} + a_6\tilde{X} + a_7\right)\tilde{Y} + \Omega_Y\right]\tilde{Y} + \Omega \tag{13}$$

where $\tilde{X} = X - X_{i,j}$ and $\tilde{Y} = Y - Y_{i,j}$. The coefficients of $a_1, a_2, \ldots, a_7$ are determined so that the interpolation function and its first derivatives are continuous at both ends. With this restriction, the numerical diffusion can be greatly reduced when the interpolated profile is constructed. The spatial derivatives are then calculated as

$$F_{X,i,j}(X,Y) = (3a_1\tilde{X} + 2a_2\tilde{Y} + a_3)\tilde{X} + (a_4 + a_6\tilde{Y})\tilde{Y} + \Omega_X \tag{14}$$

$$F_{Y,i,j}(X,Y) = (2a_2\tilde{Y} + a_3)\tilde{X} + (3a_5\tilde{Y} + 2a_6\tilde{X} + 2a_7)\tilde{Y} + \Omega_Y \tag{15}$$

In the two-dimensional case, the advected profile is approximated as follows

$$\Omega^n_{i,j} = F_{i,j}(X+\eta, Y+\xi) \tag{16}$$

$$\Omega^n_{X,i,j} = F_{X,i,j}(X+\eta, Y+\xi) \tag{17}$$

$$\Omega^n_{Y,i,j} = F_{Y,i,j}(X+\eta, Y+\xi) \tag{18}$$

where $\eta = -U\Delta\tau$ and $\xi = -V\Delta\tau$. The newly calculated spatial quantities are then used to solve the non-advection phase of Eqs. (10) to (12) and vorticity formulation of Eq. (5). In the present study, the explicit central finite different discretization method is applied with second order accuracy in space. For example, the treatment for Eqs. (5) and (10) is

$$\Omega^{n+1}_{i,j} = \Omega^n_{i,j} + \Delta\tau\left[\frac{1}{Re}\left(\frac{\Omega^n_{i+1,j} - 2\Omega^n_{i,j} + \Omega^n_{i-1,j}}{(\Delta X)^2} + \frac{\Omega^n_{i,j+1} - 2\Omega^n_{i,j} + \Omega^n_{i,j-1}}{(\Delta Y)^2}\right)\right] \tag{19}$$

$$\Psi^n_{i,j} = \frac{\frac{\Psi^n_{i+1,j}+\Psi^n_{i-1,j}}{(\Delta X)^2} + \frac{\Psi^n_{i,j+1}+\Psi^n_{i,j-1}}{(\Delta X)^2} + \Omega^n_{i,j}}{\frac{2}{(\Delta X)^2} + \frac{2}{(\Delta Y)^2}} \tag{20}$$

where superscript n represents the increment of time step and subscripts i and j represent the discretized x and y directions, respectively.

In summary, the evolution of the CIP scheme consists of three steps. The initial values of $\Omega^n_{i,j}$, $\Omega^n_{X,i,j}$ and $\Omega^n_{Y,i,j}$ are specified at each grid point. Then the system evolves in the following steps;

1. Since the pre-advected values of $\Omega^n_{i,j}$, $\Omega^n_{X,i,j}$ and $\Omega^n_{Y,i,j}$ are known on each grid, the constrained interpolation process can be completed according to Eqs. (16), (17) and (18).
2. After the interpolation, advection takes place, and $\Omega^{n*}_{i,j}$, $\Omega^{n*}_{X,i,j}$ and $\Omega^{n*}_{Y,i,j}$ are obtained.
3. The values of $\Omega^{n+1}_{i,j}$, $\Omega^{n+1}_{X,i,j}$ and $\Omega^{n+1}_{Y,i,j}$ on the mesh grid are then computed from the newly advected values in step 2 by solving the non-advection phase of the governing equation. Then the interpolation and the advection processes are repeated.

To predict the dynamics of solid particles in shear driven cavity flow, the equation of motion for a solid particle must be expressed as

$$m_p = \frac{d\mathbf{v}_p}{dt} = \mathbf{f}_p \tag{21}$$

where m_p, $\mathbf{v}_p$ and $\mathbf{f}_p$ are the mass of the particle, its velocity and drag force acting on the particle due to the surrounding fluid, respectively. This drag force can be expressed as

$$\mathbf{f}_p = C_D A_p \rho \frac{|\mathbf{u} - \mathbf{v}_p|(\mathbf{u} - \mathbf{v}_p)}{2} \tag{22}$$

where A_p is the projected area of the solid particle and C_D is the drag coefficient which is given as

$$C_D = \frac{24}{Re_p} \tag{23}$$

The particle's Reynolds number in the above equation is calculated as follows

$$Re_p = \frac{d_p|\mathbf{u} - \mathbf{v}_p|}{\upsilon} \tag{24}$$

where d_p is the diameter of the solid particle.

In the computational technique, the new value of the particles' velocity $\mathbf{v}^{n+1}_p$ can be determined since the pre-calculated value of $\mathbf{v}^n_p$ is known at the previous time step as follows

$$m_p\frac{\mathbf{v}^{n+1}_p - \mathbf{v}^n_p}{\Delta\tau} = \mathbf{f}_p \tag{25}$$

Then the new position of the solid particle can be determined as follows

$$\mathbf{x}^{n+1}_p = \mathbf{v}^{n+1}_p\Delta\tau + \mathbf{x}^n_p \tag{26}$$

4 Results and Discussion

The code was first validated against experimental results by comparing the trajectory of a particle with approximately the same density with the surrounding fluid so that the neutral buoyancy was obtained. The size of the solid particle is considered small enough and limited to not more than ten percent of the grid size. $\Delta X$and $\Delta\tau$ were set at 0.01 and 0.00015 to ensure CFL stability. For the simulation, the top lid is constantly moved so that the resultant Reynolds number is 470 as in Tsorng et al. [18]. In their report, Tsorng et al. discussed a three-dimensional measurement of a particle suspended in a fluid enclosed in a transparent cubic cavity. Before the experiments, the particle was plunged into the cavity so that it touched the lid and its initial location was approximately in the middle below the lid. Figure 1 shows the comparison between numerical solution and experimental work as a trajectory of the particle.

For the first few seconds, both the numerical and the experimental results match very closely. Nevertheless, after this time, some deviations were noticeable due to the following reasons:

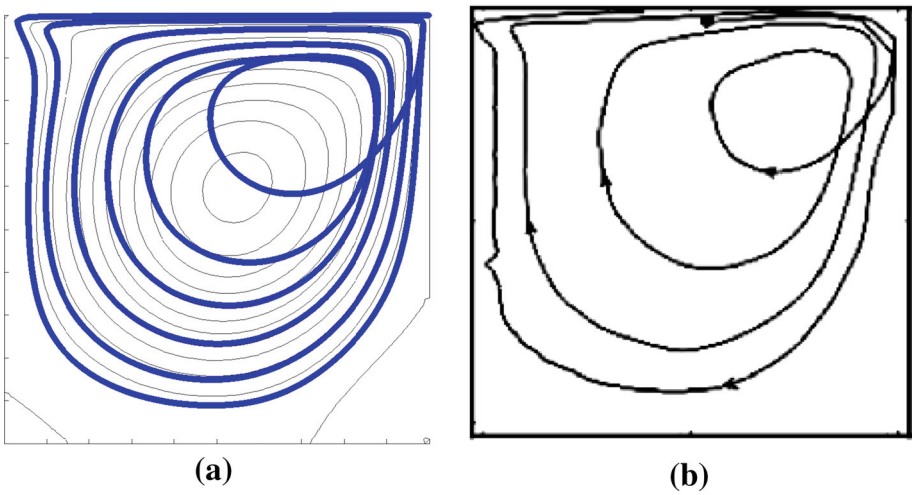

Fig. 1 Particle's trajectory for $Re = 470$ obtained from **a** present computation (*thin lines* represent the streamline at steady state) and **b** experimental results [18]

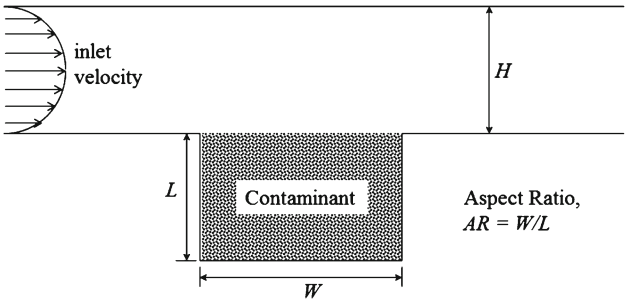

Fig. 2 Physical domain of the problem

1. As our numerical approach considered a two-dimensional investigation, it cannot perfectly match with the actual flow which is in three dimensions once it exceeds a certain period of time.
2. It is almost impossible to precisely determine the particle's initial position due to the sophistication of the fluid flow structure.
3. The presence of lubricant between the conveyer and fluid affects the shear strength on the fluid surface and causes slight deviations in terms of Reynolds number.

In our next predictions, one of the physical domains of the problem is set as demonstrated in Fig. 2. The other two cavity shapes, i.e semicircular and triangular, located on the floor of horizontal channel, will also be considered in the present study. The same number of meshes was used for all cases. Since we applied very small spatial resolution, the semicircular shape can be well reproduced even with the Cartesian coordinate. The maximum inlet velocity was varied to give the Reynolds number ranges from 100 to 400. A swamp of solid particle was initially filled in the cavity as shown in the figure. In the present analysis, the computations are conducted on a two-dimensional plane. This two-dimensional approximation was undertaken based on a physical assumption that the behavior of the vortex is relatively unaffected by the three dimensionality of the flow for this range of Reynolds numbers.

Figures 3, 4, 5 show the process of solid particles removal from three different cavity shapes with width to depth ratio of $W/L = 2$. The cavities were initially filled up with solid particles of the same amount. As demonstrated by the figures, the highest rate of removal occurred on the early penetration of fluid flow into the cavity. This was due to the early development of a vortex, which penetrated into the cavity and flushed the contaminant out of the cavity. Then, when this recirculation area was shaped in the cavity, it trapped some of the contaminant particles and remained in the cavity until steady state was achieved. The shape of the cavity and Reynolds number also had significant effects on the percentage of particle removal from the cavity. These are presented in Fig. 6, where the comparisons are made for all the cases.

As can be seen from Figs. 6, 7, 8, the removal percentage is clearly dependent on the Reynolds number for all cavity shapes. A higher value of Reynolds number results in higher speed of flow velocity inside the cavity and deeper penetration of the vortex into the cavity. This will drag the solid particles to the lower region inside the cavity and due to the inertia force, these particles are flushed out from the cavity to the downstream channel.

To see more details about the effect of cavity geometry on the efficiency of contaminant removal, we plotted the comparison of removal percentage for different shapes of cavity and demonstrated in Figs. 9, 10, 11. At low Reynolds number simulation, the circulation region is symmetric for all cases and its vortex center is located in the center of the cavity. However, due to shallow cavity depth for the case of triangular cavity, this shape was able to remove the highest percentage of contaminant compared to the two other cavities. When

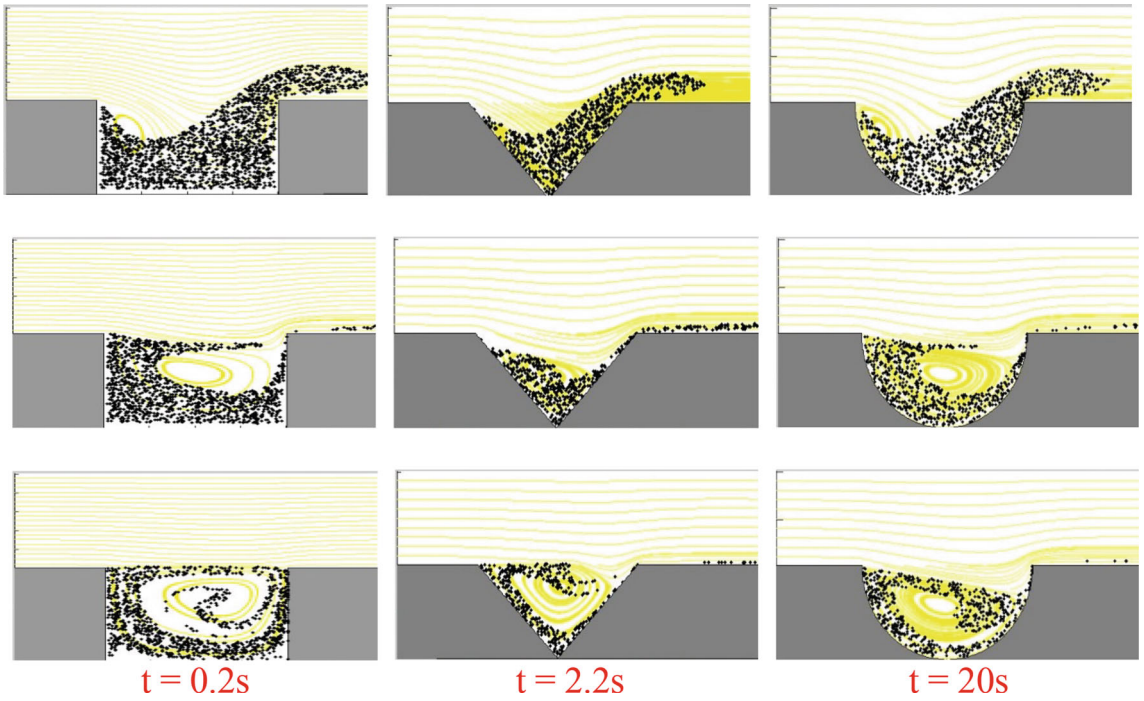

Fig. 3 Snapshots of contaminant removal from cavities at $Re = 50$

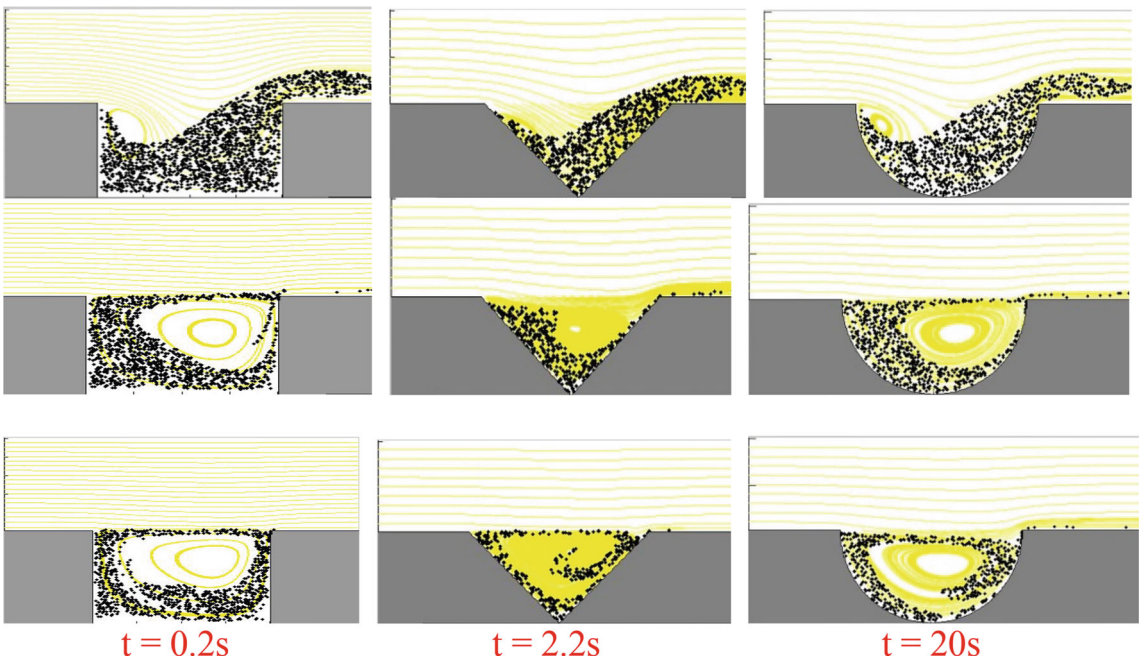

Fig. 4 Snapshots of contaminant removal from cavities at $Re = 100$

the Reynolds number is increased, the center of the vortex moves to the upper right edge of the cavity for the triangular and semicircular cavities while it remains in the center of the cavity for the rectangular cavity case [7]. This feature of vortex dynamics contributes to great effect on the efficiency of contaminant removal from the cavity as shown in Fig. 10. When the vortex was formed in the cavity, it trapped the solid particles, and as it moved to the upper region, it

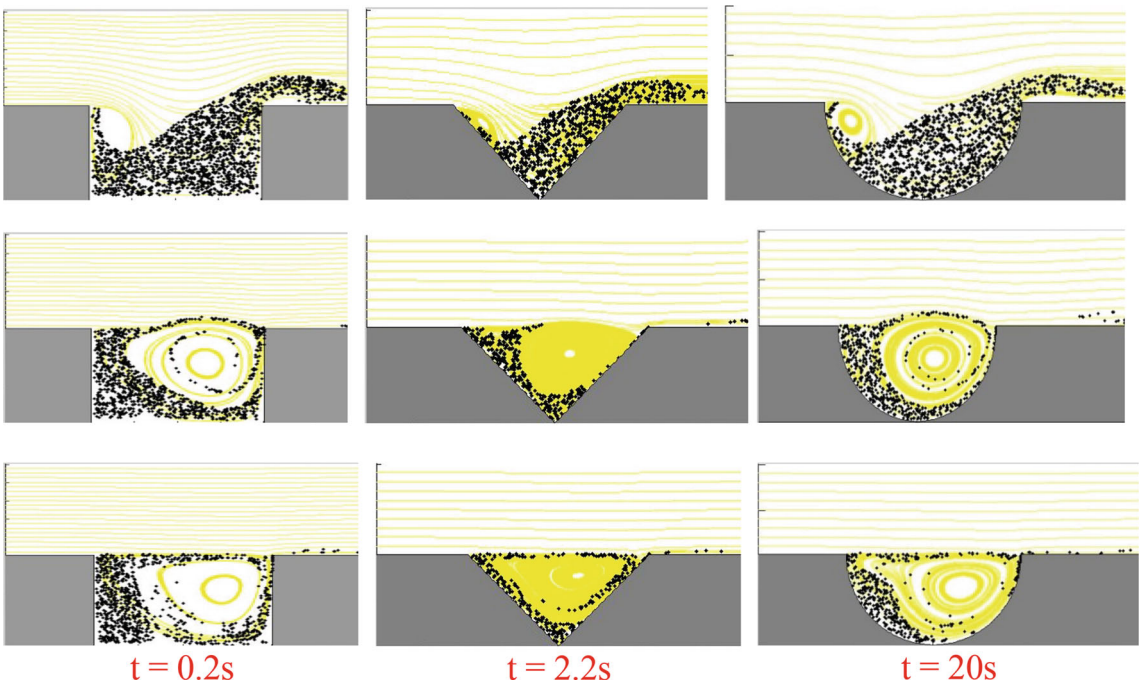

Fig. 5 Snapshots of contaminant removal from cavities at $Re = 400$

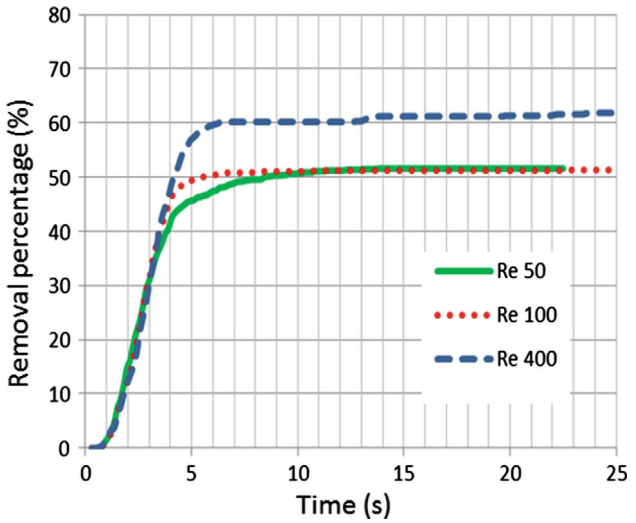

Fig. 6 Particle removals from triangular cavity at different Reynolds numbers

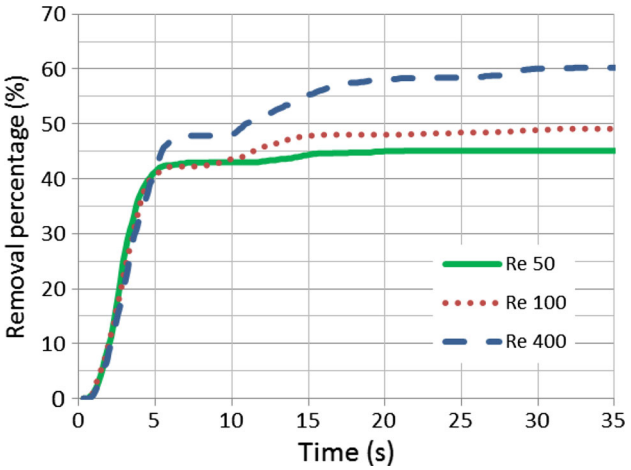

Fig. 7 Particle removal from semicircular cavity at different Reynolds numbers

brought along the trapped particle and flushed it out from the cavity by the centrifugal force to the downstream part of the channel. This explained the high percentage of removal by the triangular and semicircular cavities of Fig. 11. However, the graphs show some delay in the removal percentage for the semicircular case compared to the triangular case. This was explained by Ozalp that the vortex in a semicircular cavity takes longer time to propagate to the upper right region compared to the triangular case. This also explains the gradual increment of contaminant removal from semicircular and rectangular cavities after around 6 s of simulation.

For all cases, we can see in a steady state condition, the remaining particles are trapped near the boundaries of the cavity. These particles can be further removed by introducing the buoyancy force on the particles. This can be done by heating up the bottom of the cavity to induce diffusion effect on the fluid as proposed by Chilikuri and Middleman [33]. Further discussion on this subject will be our next research topic.

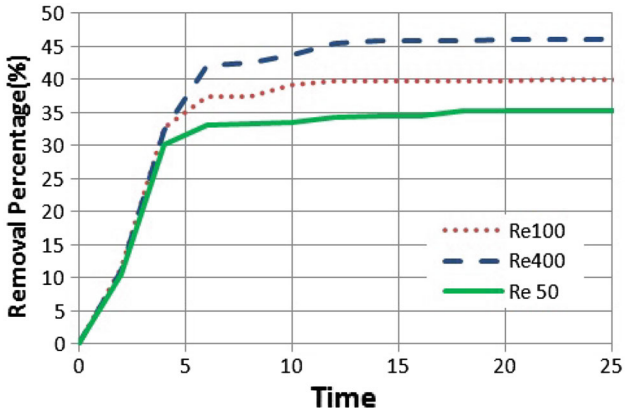

Fig. 8 Particle removal from rectangular cavity at different Reynolds numbers

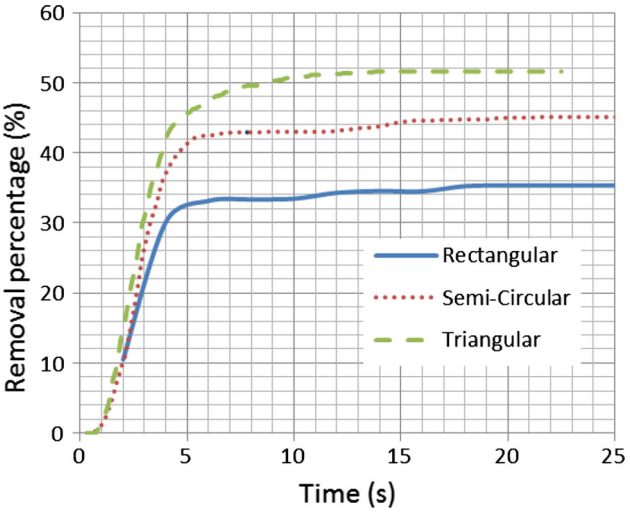

Fig. 9 Particle removal from cavities at Reynolds numbers of $Re = 50$

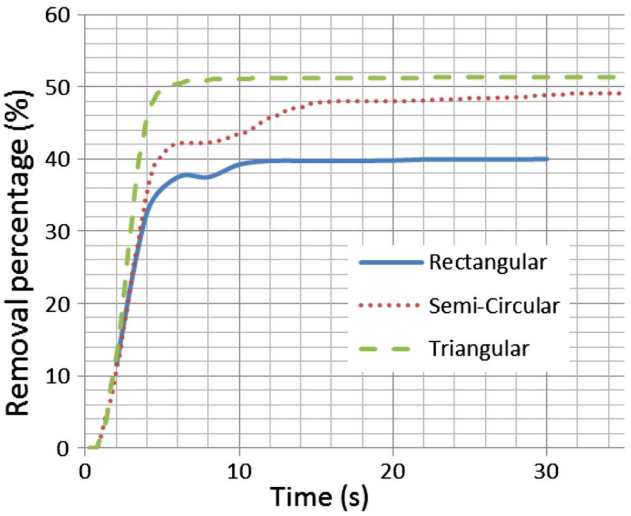

Fig. 10 Particle removal from cavities at Reynolds numbers of $Re = 100$

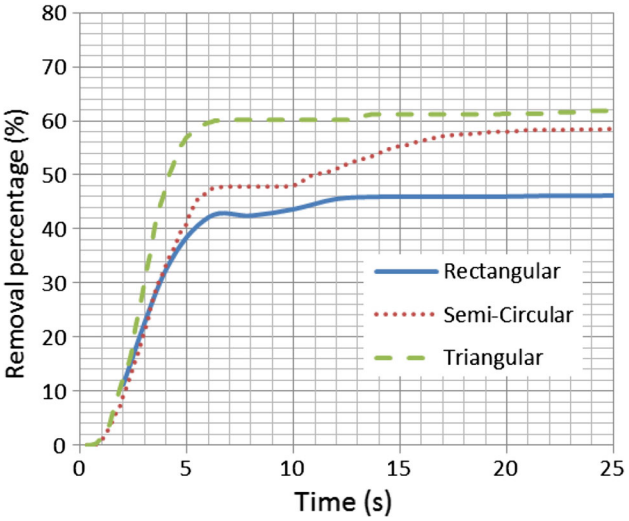

Fig. 11 Particle removal from cavities at Reynolds numbers of $Re = 400$

5 Conclusion

The flow structure and rate of solid particle removal were obtained for three different shapes of cavity and three different Reynolds numbers using a state of the art numerical technique, namely CIP. The primary goal of this study is to investigate the effect of cavity shapes on the characteristics of the flow within the cavities and the particle dynamics in the cavity. The results of the work presented in this study reveal that, in addition to cavity shapes, Reynolds number changes have some degree of influence on the structure of flow and the rate of particle removal. Snapshots of the particle dynamics indicate that the highest rates of removal occur in the early penetration of flow into the cavity, especially for the triangular cavity. These demonstrate the capability and the multidisciplinary applications of the present numerical scheme. Future efforts need to extend the current formulation for investigation at various types of solid–fluid flow related to real engineering problems.

Acknowledgments The authors wish to acknowledge Universiti Teknologi Malaysia and Malaysia government for supporting these research activities.

References

1. Hayashi, H.; Kubo, S.: Computer simulation study on filtration of soot particles in diesel particulate filter. Comp. Math. App. **55**(7), 1450–1460 (2008)
2. Rockwell, D.; Lin, J.C.; Oshkai, P.; Reiss, M.; Pollack, M.: Shallow cavity flow tone experiments: onset of locked-on states. J. Fluids. Struct. **17**(3), 381–414 (2003)
3. Xu, B.H.; Yu, A.B.: Numerical simulation of the gas-solid flow in a fluidized bed by combining discrete particle method with computational fluid dynamics. Chem. Eng. Sci. **52**(16), 2785–2809 (1997)

4. Mesalhy, O.M.; Abdel Aziz, S.S.; El- Sayed, M.M.: Flow heat transfer over shallow cavities. Int. J. Thermal Sci. **49**(3), 514–521 (2010)
5. Zdanski, P.S.B.; Ortega, M.A.; Nide, G.C.R., Fico, J.: On the flow over cavities of large aspect ratio: a physical analysis. Int. Commun. Heat Mass Transf. **33**(4), 458–466 (2006)
6. Kang, W.; Sung, H.J.: Large-scale structures of turbulent flows over an open cavity. J. Fluids Struct. **25**(8), 1318–1333 (2009)
7. Ozalp, C.; Pinarbasi, A.; Sahin, B.: Experimental measurement of flow past cavities of different shapes. Exp. Thermal Fluid Sci. **34**(5), 505–515 (2010)
8. Li, S.L.; Yi, C.C.; Chao, A.L.: Multi relaxation time lattice Boltzmann simulations of deep lid driven cavity flows at different aspect ratios. Comput. Fluids **45**(1), 233–240 (2011)
9. Arlindo, D.M.; Francisco, A.A.P.; Aristeu, S.N.: Large-eddy simulation of turbulent flow over a two dimensional cavity with temperature fluctuations. Int. J. Heat Mass Transf. **42**(1), 49–59 (1999)
10. Stiriba, Y.: Analysis of the flow and heat transfer characteristics for assisting incompressible laminar flow past an open cavity. Int. Commun. Heat Mass Transf. **35**(8), 901–907 (2008)
11. Yapici, K.; Karasozen, B.; Uludag, Y.: Finite volume simulation of viscoelastic laminar flow in a lid- driven cavity. J. Non Newton. Fluids Mech. **164**(1), 51–65 (2009)
12. Yang, Y.; Rockwell, D.; Cody, K.L.F.; Pollack, M.: Generation of tones due to flow past a deep cavity: Effect of streamwise length. J. Fluids Struct. **25**(2), 364–388 (2009)
13. Ekmekci, A.; Rockwell, D.: Oscillation of shallow flow past a cavity: Resonant coupling with a gravity wave. J. Fluids Struct. **23**(6), 809–838 (2007)
14. Zaki, M.M.; Nirdosh, I.; Sedahmed, G.H.: Mass transfer inside conical cavities under transverse laminar flow. Chem. Eng. Process. Process Intensif. **44**(12), 1306–1311 (2005)
15. Fang, L.C.; Nicolaou, D.; Cleaver, J.W.: Transient removal of a contaminated fluid from a cavity. Int. J. Heat Fluid Flow **20**(6), 605–613 (1999)
16. Patil, D.V.; Lakshmisha, K.N.; Rogg, B.: Lattice Boltzmann simulation of lid-driven flow in deep cavities. Comput. Fluids **35**(10), 1116–1125 (2006)
17. Stiriba, Y.; Grau F.X.; Ferre J.A.; Vernet, A.: A numerical study of three-dimensional laminar mixed convection past an open cavity. Int. J. Heat Mass Transf. **53**(21), 4797–4808 (2010)
18. Tsorng, S.J.; Capart, H.; Lai, J.S.; Young, D.L.: Three-dimensional tracking of the long time trajectories of suspended particles in a lid-driven cavity flow. Exp. Fluids **40**(2), 314–328 (2006)
19. Adrian, R.J.: Particle-imaging techniques for experimental fluid mechanics. Ann. Rev. Fluid Mech. **23**(1), 261–304 (1991)
20. Han, M.; Kim, C.; Kim, M.; Lee, S.: Particle migration in tube flow of suspensions. J. Rheo. **43**(5), 1157–1174 (1999)
21. Matas, J.P.; Morris, J.F.; Guazzelli, E.: Inertial migration of rigid spherical particles in Poiseuille flow. J. Fluid Mech. **515**(1), 171–195 (2004)
22. Ushijima, S.; Tanaka, N.: Three-dimensional particle tracking velocimetry with laser-light sheet scannings. Fluid Eng. **118**(2), 352–357 (1996)
23. Ide, K.; Ghil, M.: Extended Kalman filtering for vortex system. Dyn. Atm. Oceans **27**(1), 301–332 (1997)
24. Hu, C.C.: Analysis of motility for aquatic sperm in videomicroscopy, PhD. Thesis, National Taiwan University, Taiwan (2003)
25. Liao, J.I.: Trajectory and velocity determination by smoother, PhD Thesis, National Taiwan University, Taiwan (2002)
26. Kosinki, P.; Kosinska, A.; Hoffmann, A.F.: Simulation of solid particles behavior in a driven cavity flow. Pow. Tech. **191**(3), 327–339 (2009)
27. Ilea, C.G.; Kosinski, P.; Hoffmann, A.C.: Three-dimensional of a dust lifting process with varying parameters. J. Multiph. Flow **34**(9), 869–878 (2008)
28. Kosinski, P.; Hoffmann, A.C.: An extension of the hard-sphere particle-particle collision model to study agglomeration. Chem. Eng. Sci. **65**(10), 3231-3239 (2010)
29. Takewaki, H.; Nishigushi, A.; Yabe, T.: Cubic interpolated pseudo particle method for solving hyperbolic type equations. J. Comput. Phys. **61**(2), 261–268 (1985)
30. Nor Azwadi, C.S.; Mohd Rosdzimin, A.R.; Al-Mola, M.H.: Contrained interpolated profile for solving BGK Boltzmann equation. Eur. J. Sci. Res. **35**(4), 559-569 (2009)
31. Yabe, T.; Aoki, T.: A universal solver for hyperbolic equations by cubic-polynomial interpolation I. One-dimensional solver. Comput. Phys. Commun. **66**(2), 219–232 (1991)
32. Nor Azwadi, C.S.; Mohd Rosdzimin, A.R.: Cubic interpolated pseudo particle (CIP)—thermal BGK lattice Boltzmann numerical scheme for solving incompressible thermal fluid flow problem. Malay. J. Math. Sci. **3**(2), 183–202 (2009)
33. Chilukuri, R.; Middleman, S.: Circulation, diffusion and reaction within a liquid trapped in a cavity. Chem. Eng. **22**(3), 127–138 (1983)